Send Orders for Reprints to reprints@benthamscience.net

The Open Materials Science Journal, 2014, *8*, 18-26

Open Access

High Temperature Corrosion Resistance of Pt-Based Superalloys in 0.2% SO_2 -N_2 Gas

Johannes H. Potgieter* and Nthabiseng B. Maledi

NRF/DST Centre of Excellence in Strong Materials, School of Chemical and Metallurgical Engineering, University of the Witwatersrand, Private Bag 3, WITS, 2050, South Africa

Abstract: Pt-based superalloys are a new generation of materials intended to be used in various high temperature applications. Effluent gases emitted to the environment during combustion operations can lead to degradation of high temperature materials with deleterious effects on mechanical integrity and the corrosion of alloys. This paper focuses on sulphidation of one quaternary, and four ternary, Pt-based superalloys of various chemical compositions. Pt-based superalloys were exposed at 900°C in a reducing environment. The alloys were compared to coated and uncoated Ni-based superalloys (NBSAs). X-Ray diffraction (XRD), Scanning electron microscopy (SEM) and Raman spectroscopy were used to characterize corrosion products that formed. The Pt-based superalloys exhibited higher corrosion resistance than NBSAs as a result of the formation of a protective Al_2O_3 scale, whereas NBSAs suffered internal sulphidation and formed Cr and Ni sulphide corrosion compounds. The formation of brittle needle-like phases and the transformation of the NiAl phase to Ni_3Al, led to early failure of the coated alloy. Pt-based superalloys alloyed with Co showed poor corrosion resistance as a result of depletion of alloying elements.

Keywords: Alumina, chromium, corrosion, high temperature, metals, NBSA, Pt-based superalloys, sulphidation.

INTRODUCTION

Superalloys are complex engineering materials with a unique combination of properties (high strength and good resistance to creep, fatigue and oxidation resistance, etc.) used in demanding high temperature applications such as gas turbines in the aerospace and land based engines, waste incinerators, fossil-fired steam boilers, the power generation industry and paper and pulp industries [1]. Superalloys are classified into three main classes based on the group VIIIA elements, Fe, Co and Ni. Nickel-based superalloys are the most popular amongst the superalloys, and find their largest application in the production of aero-engine turbine blades, constituting over 50% of the materials found in the gas turbine engine [2].

The need for increased operating temperatures in gas turbines has revolutionised the gas turbine industry since its development in the 1940s. Early age gas turbine engines were designed to operate at 700ºC. Improvements in metallurgical processes, from vacuum casting, through to single crystal casting, advanced cooling and application of coatings, all contributed towards increasing working temperatures [3-6]. The continued improvements in the aerospace gas turbine industry subsequently also benefited the land based gas turbine industry [7], and currently land based turbines are fast approaching the efficiencies achieved in the aerospace engines. Today's gas turbines are operating at 1100ºC. In addition, there is a demand to further increase the working temperatures to 1350°C [4]. Increases in inlet gas turbine temperatures benefit the gas turbine industry by allowing for improved efficiencies, reduction in fuel consumption and a greener environment, because of a reduction in the levels of CO_2 and hydrocarbon emissions [8,9].

An increase in high temperature strength by increasing the Al and reducing the Cr content resulted in alloys that are more susceptible to high temperature corrosion. Poor corrosion resistance by the high temperature materials led to the development and introduction of coatings [10,11]. Today, it is common practice to apply coatings to gas turbine hot section components, because coatings (e.g. thermal barrier coatings, overlay coatings and diffusion coatings) have the capability to withstand temperatures exceeding the substrate melting temperature, while simultaneously reducing the incoming temperatures and protecting the substrate from environmental degradation [12].

Unfortunately, these desired working temperatures are excessively high for NBSAs to withstand [13]. NBSAs are currently operating at near melting point temperatures [3,14-16]. Further temperature increases would result in the dissolution of the strengthening phase and subsequent melting of the alloy. Alternatively, new materials with higher melting temperatures, high strengths and good corrosion resistance could be employed to replace NBSAs [14,15]. Fischer *et al*. [17] stated that problems encountered in the aerospace industry could be solved by using Pt-based alloys, because they have proved to do exceptionally well in various high temperature applications, including areas such as glass manufacturing, handling of corrosive substances, etc.

*Address correspondence to this author at the NRF/DST Centre of Excellence in Strong Materials, School of Chemical and Metallurgical Engineering, University of the Witwatersrand, Private Bag 3, WITS, 2050, South Africa; Tel: 0027 11 717 7510;
E-mail: johannes.potgieter@wits.ac.za

1874-088X/14

[18,19]. This idea was further extended by Wolff, who proposed that Pt-based alloys, with similar structures to NBSAs, could be developed to benefit the aerospace industry [20].

During high temperature materials development, high temperature strength is the primary, most desired property [14]. Other properties that require attention are creep and high temperature corrosion resistance [21,22]. These properties become significant with increasing temperatures, hence it is imperative that during the materials selection process, corrosion evaluations be taken into consideration. Apart from serious catastrophic failures, corrosion/oxidation has a serious economic impact. Significant amounts of money are spent annually on corrosion related problems, therefore better corrosion control technologies can largely contribute towards saving money and extending the operational life of the alloys [23].

High temperature corrosion becomes significant with increasing temperatures. Moreover, traces of impurities commonly found in fuels or ingested air, such as Na, S, V, etc. impact negatively on corrosion properties, by forming solid deposits such as Na_2SO_4. Na_2SO_4, NaCl and other sulphate salts which are corrosive in nature when they are in their molten state and lead to a process called hot corrosion [20]. Hot corrosion is accelerated oxidation degradation of high temperature materials in the presence of fused salts or corrosive gases, and affects the mechanical integrity of alloys, reducing component life.

The Pt-based superalloys selected for this investigation were based on the Pt-Al-Cr, Pt-Al-Co and Pt-Al-Ru ternary systems. They can have at least two forms of the precipitate phases: the ordered $L1_2$ phase at high temperatures and the tetragonal DO_C' phase at low temperatures. A comprehensive discussion of these phase formations and their influence on the mechanical properties of Pt-based superalloys can be found in Cornish *et al*. [24]. The high temperature precipitate form was stabilised by adding Cr, Ti and Ta [25]. The optimum alloy selected for this investigation was based on the quaternary alloy system (Pt-Al-Cr-Ru), and is a fine two-phase mixture. Additionally, this alloy yielded the best oxidation properties during isothermal oxidation tests and possesses a reasonable hardness of 472 ± 14 HV_{10} [26], compared to other ternary Pt-based alloys, such as Pt_{86}:Al_{10}:Cr_4 ($317HV_{10}$) and Pt_{86}:Al_{10}:Ru_4 ($278HV_{10}$)[27].

This investigation focused on type I hot corrosion since it is commonly found in aircraft. Type I hot corrosion is commonly observed at around 850ºC to 950ºC, while type II hot corrosion typically occurs at 650ºC to 800ºC. The emphasis of the current work was to evaluate the oxidation behaviour of Pt-based superalloys and to identify the best performing alloys for potential commercial application in the gas turbine industry. In the evaluation process, Pt-based superalloys were ranked and compared to commonly used NBSAs. Pt-based superalloys were exposed to corrosive environments containing sulphur dioxide at high temperatures to determine the effect of sulphur on the behaviour of the developed high temperature materials and the occurrence and severity of sulphidation. The results of this investigation can contribute to increased applications of Pt superalloys in high temperature environments.

EXPERIMENTAL PROCEDURES

Materials

Five Pt-based superalloys button samples of approximately 2 g were prepared by weighing out masses of elements, in their purest form (99.9%), equivalent to the chemical compositions of the alloys. These elements were arc-melted under an argon atmosphere. The alloys were turned several times to provide homogeneity in the alloys. The choice of alloying additions was based on the fact that Cr stabilises the cubic Pt_3Al precipitates, Al accelerates oxide scale formation [28], Ru acts as solid solution strengthener [16] and Co enhances the alloy's formability [29]. The hot corrosion behaviour of four ternary and one quaternary Pt-based superalloys, with chemical compositions given in Table **1**, were tested and compared with two single crystal alloys, a coated and an uncoated CMSX-4 nickel-based superalloy. The nominal chemical composition of the benchmark alloy, CMSX-4, is also included in Table **1**. A thin aluminide coating of approximately 1 μm thickness was applied on one of the benchmark alloys.

Weight change methods were employed to assess the performance of the alloys. Prior to the tests, exposed surfaces of the samples were abraded on silicon carbide paper in succession from 200, 600, up to 1000 grit finish. Samples were rinsed and degreased in acetone and dried.

Sulphidisation Test

During sulphidation tests, alloys were exposed to a controlled reducing environment. Samples were exposed to a pre-mixed special gas mixture of 0.2% SO_2-N_2. The gas was first allowed to flow through oil to remove moisture and then

Table 1. Nominal chemical compositions of selected Pt-based superalloys (at. %).

Alloys	Pt	Al	Cr	Ru	Co	
RS-1	86	10	4	-	-	
RS-2	86	10	-	4	-	
RS-3	84	11	3	2	-	
P420	79	15	-	-	6	
P421	73	15	-	-	12	
	Ni			Mo		W/Ta/Ti
CMSX-4	66.4	11.5	6.5	0.3	11	1.7/1.8/0.9

charged into a horizontal, electric tube furnace preheated to 900°C. The gas leaving the furnace was flowed through oil before venting the gas to the atmosphere. The air in the furnace was purged by allowing the mixed gas to flow for approximately 15 minutes at the specified temperature, prior to placing samples in the test chamber. Each test was run for a total of 60 hours, with cycles of 5 hours of heating, followed by furnace cooling under a nitrogen atmosphere to room temperature. At the end of each cycle, weight changes were recorded and the samples were placed back into the furnace.

Materials Characterisation

Materials characterisation involved non-destructive tests such as scanning electron microscopy with energy dispersive analyses (EDX), X-ray diffraction, Raman spectroscopy, and optical microscopy (OM) to evaluate corrosion products and deduce the corrosion mechanism.

Scanning Electron Microscopy with X-Ray Energy Dispersive Spectrometry

A JEOL 840 scanning electron microscope was used to identify the oxidation products' morphology and study the cross sectional analysis of the alloys, using a voltage of 20 kV. Semi-quantitative and qualitative analyses were determined from using EDX.

X-Ray Diffraction

A Phillips-PW1710 XRD spectrometer was used to identify the oxidation products that formed on the surfaces of the seven alloys. Generator settings for the analysis were set at 40 kV and 20 mV with copper K-alpha as the anode. A scan with a step size of 0.02° per minute was run from a starting position of 10° up to 100° (2θ). Expert High Score software was used to identify peaks in each of the spectra.

Raman Spectroscopy

A JOBIN-YVON T64000 Raman spectrometer was used in the investigation to identify thin surface films on the samples. The spectrum was collected by directing a continuous laser of Ar^+ (514.5 nm) on the alloy surface at room temperature. The spectrum covered a scanning range between 250 cm^{-1} and 2500 cm^{-1}.

Optical Microscopy

An Axiocam microscope installed with the Axio vision 3.1 programme was used to study the cross sections of the corroded sample. Low magnifications up to 50X were employed.

RESULTS AND DISCUSSION

Corrosion Kinetics Obtained After Sulphidation

Fig. (**1**) gives the oxidation curves of the investigated alloys after being exposed to mixed gases at 900ºC for a period of 60 hours. Mass change were calculated as the mass at any time t minus the initial mass (at time t=0). It was observed that the mass changes over time were the highest for the coated alloy. Rapid mass change was observed on the uncoated alloy, which experienced weight gain during the initial stages of the experiment, followed by a relatively constant behaviour. It has to be taken into account that due to very small mass changes within the measurement limit of the balance used, fluctuations in the mass chances were encountered. Minimal mass changes were attributed to the formation of oxidation products that acted as a barrier, making it difficult for elements and the gas to diffuse inwards or outwards. Fluctuations in mass gains were very noticeable in alloys P420 and P421. Instability by Co-containing alloys after exposure to corrosive gases indicates poor oxidation resistance of the alloys. Alloy RS1, RS2 and RS3 were reasonably stable with little changes in mass, with alloys RS2 and RS3 recording the lowest mass changes.

There are essentially three groups of alloy compositions among the seven alloys investigated, i.e. Pt alloys containing either Cr, Ru or both, Pt alloys containing various amounts of Co, and the base NBSA with and without an aluminide coating. Each alloy has been analysed by SEM/EDX, XRD, optical microscopy and Raman spectroscopy, and similarities as well as differences in their observed oxidation behavior will be highlighted.

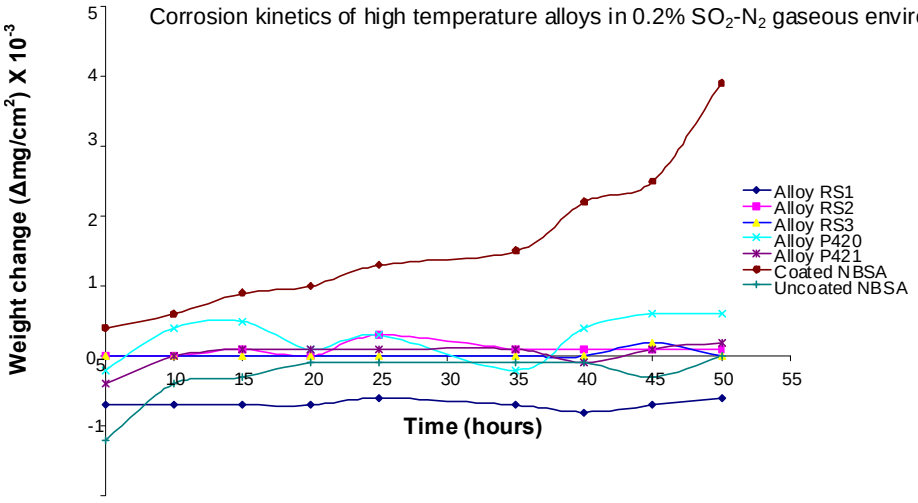

Fig. (1). Corrosion of the seven investigated alloys after sulphidation in a 0.2% SO_2-N_2 gaseous environment.

The Pt-Al-Cr-Ru Alloys

Cross-sectional examinations of the corroded sections of the investigated alloys were evaluated using a high resolution electron microscope. The attack on the surface of Alloy RS1 was not uniform throughout. Fig. (**2a**) shows the affected corroded area showing internal oxidation that was approximately 2 µm deep. A fine dispersion of precipitates randomly distributed in the alloy was also seen in the substrate. No sulphides were detected on the corroded area. However, it was observed that a thin layer of alumina was formed on the external surface of the alloy, as was confirmed by the EDX analysis shown in Fig. (**2b**). The formation of Al_2O_3 scale led to the depletion of the alloying elements that resulted in a Pt-rich area. Cr was in low concentration, and at these working temperatures, it was likely that Cr oxidised, forming volatile compounds.

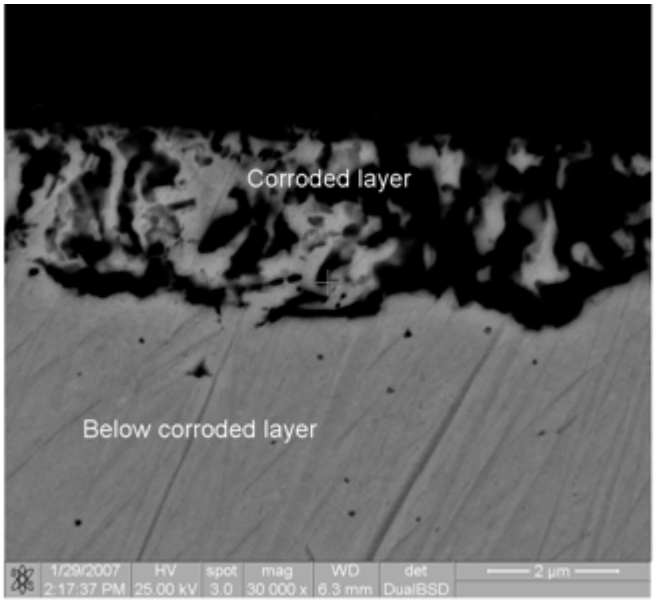

Fig. (2a). Secondary electron images of the cross-section of Alloy RS1 at 30,000X magnifications after sulphidation, showing the effect and depth of attack by 0.2% SO_2-N_2 gas.

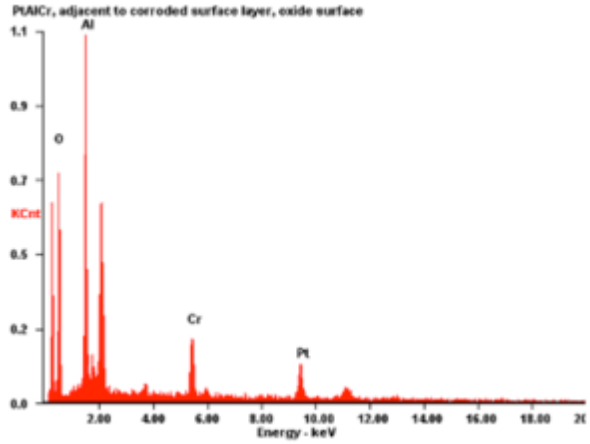

Fig. (2b). EDX analysis performed on the external scale that formed on the surface of Alloy RS1 after sulphidation in 0.2% SO_2-N_2 environment.

Insignificant changes were observed on the external surface of Alloy RS2 when the alloy was viewed under the electron microscope. The alloy was unattacked and appeared homogenous and continuous throughout with no internal oxidation, as is shown in Fig. (**3a**, **b**). This was exceptional behaviour displayed by a Pt-based superalloy.

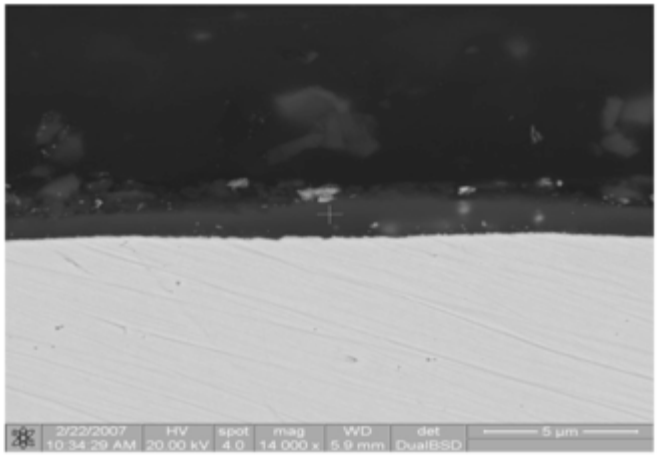

Fig. (3a). Cross-section of Alloy RS2 at 14,000X magnification with an Al_2O_3 scale forming on the surface of the alloy.

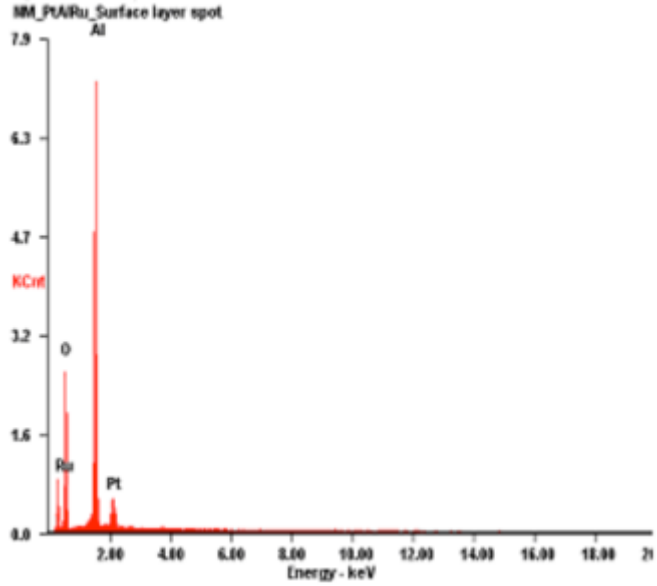

Fig. (3b). EDX analysis of the external scale of Alloy RS2.

Alloy RS3 suffered internal oxidation with possible cracks forming. The depth of attack was approximately 5 µm, and is depicted in Fig. (**4a**). The area below the thin oxide scale has lost mechanical integrity. EDX analysis of the oxide scale is given in Fig. (**4b**). Fig. (**4c**) represents XRD spectra obtained on the surface of Alloy RS3. According to the analysis, some of the oxidation products that were detected, were Al_2O_3 and the Pt_2Al phase. This is typical of what has been observed in the XRD spectra both the RS1 and RS2 also.

In summary, it seems that the Pt-Al-Cr-Ru alloys are well resistant against sulphidation, and this is due to the formation of a protective alumina film formed on the surfaces of these

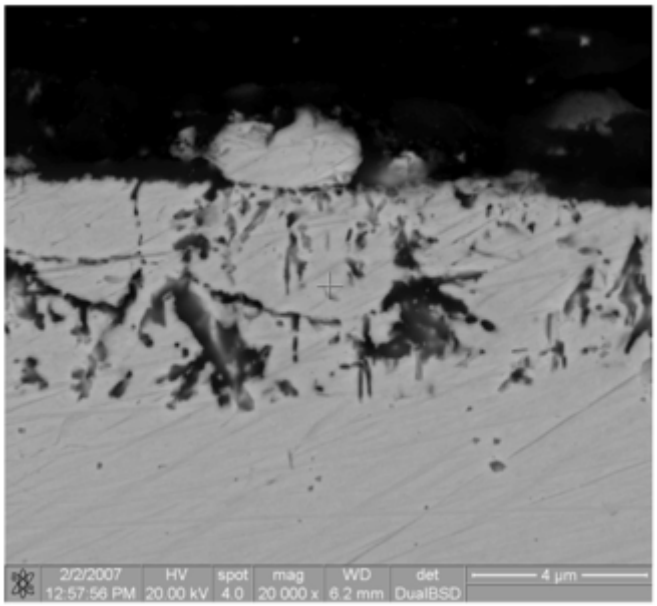

Fig. (4a). Secondary image of cross-section of Alloy RS3 after sulphidation.

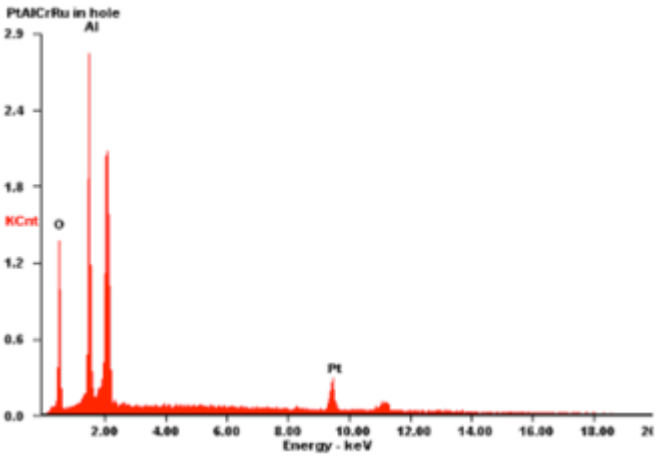

Fig. (4b). EDX analysis of the dark area in the corroded section on Alloy RS3.

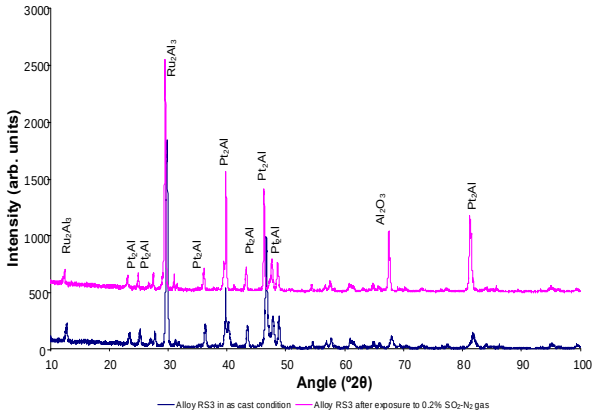

Fig. (4c). XRD spectrum performed on the external surface of Alloy RS3 [Pt-Al-Cr-Ru] before (blue) and after (pink) exposure to a 0.2% SO_2-N_2 atmosphere at 900ºC for 60 hours.

alloys. The quarternary Pt alloy displayed the poorest resistance against sulphidation attack.

The Pt-Al-Co Alloys

Oxidation characteristics of Alloys P420 and P421 were nearly similar, due to the alloys' similar chemistry. A transverse section of Alloy P420 indicated in Fig. (**5a**) shows that the attack was non-uniform across the surface of the alloy and the Al_2O_3 that formed was discontinuous. Below the corroded surface is a single area rich in Pt. The Pt-rich area is depleted of alloying elements, and a dendritic structure formed below the Pt-rich area as depicted in Fig. (**5b**). Co-containing alloys were more susceptible to corrosion attack compared to other Pt-based superalloys. Images that were taken across the surface of Alloy P421 showed similar behavior to Alloy P420. However, the corroded band was thicker than the one observed in Alloy P420, suggesting that Alloy P421 is less resistant to corrosion attacks compared to Alloy P420. Cobalt-oxides were detected on the surface of these alloys after the sulphidation test, as indicated in Fig. (**5c**). Alloy P421 underwent sulphidation and formed sulphides such as Al_2S_3 and PtS.

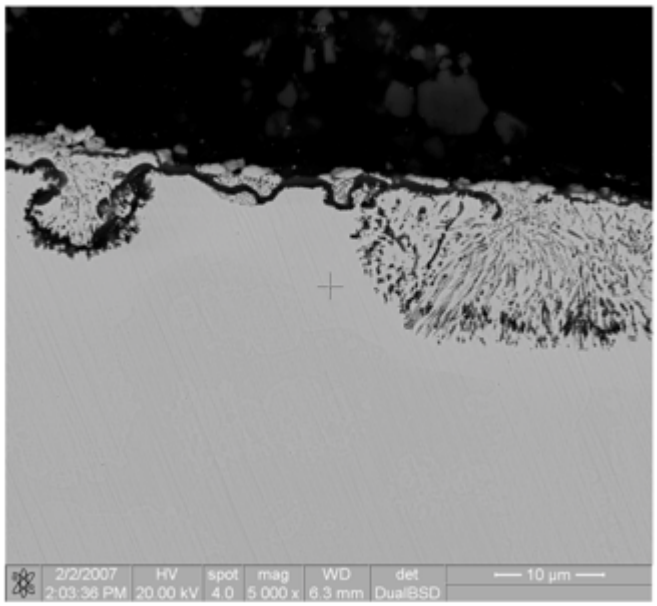

Fig. (5a). Secondary image of Alloy P420 after sulphidation in 0.2% SO_2-N_2 environment.

The NBSA Group

Variations across the transverse section of the coated alloy observed in Fig. (**6a**) indicate that there were four different sections that formed. The external area of the coated alloy consisted of a single component that comprised mainly of Al_2O_3 on its external surface, as is confirmed by the EDX analysis shown in Fig. (**6b**).

The interdiffusion zone in Fig. (**7a**) showed that needle-like structures were formed. An EDX analysis, shown in Fig. (**7b**), indicated that these needle-like structures were rich in refractory elements. The effect of sulphur on the oxidation behaviour of these alloys was the main focus of the study. It was noted that only the area below the alumina scale was affected by sulphur, where Cr_xS_y and Ni_xS_y

compounds formed. Further analysis indicated that there were no traces of S deeper into the substrate. Distinct areas were observed and the EDX analysis shown in Fig. (**7c**) indicated that instead of alumina, the alloy formed a non-protective columnar structure of NiO. Below the NiO scale was a greyish area rich in Cr.

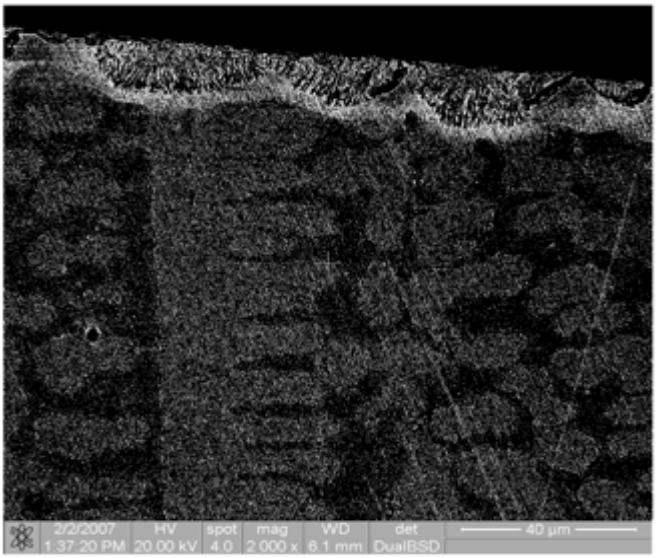

Fig. (5b). Secondary electron image of Alloy P420 with the dendritic structure below the corroded area.

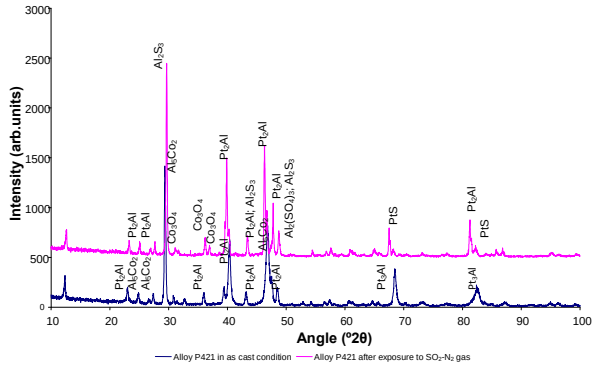

Fig. (5c). XRD pattern of Alloy P421 in as-cast condition (blue) and after (pink) exposing the alloy to a gaseous environment of 0.2% SO_2-N_2 for 60 hours.

In summary, the NBSA alloy group showed substantially poorer resistance against sulphidation than any of the two other groups evaluated. While an alumina coating seem to be the main reason why the two other groups of Pt-based alloys have excellent to reasonably good resistance against sulphidation attack, a similar layer that forms in the case of the coated and uncoated NBSAs offered no protection against further attack to the underlying substrate material.

Raman Analysis

Raman analyses were performed on surfaces of the sulphidised alloys to validate the compounds previously found. Raman scans covered a range from 250-2500 cm^{-1}. The optical micrographs of corroded surfaces are placed next to each respective spectrum of the investigated alloys. The spectra are shown in Figs. (**8-14**). Although the spectra collected at different locations were slightly different for a given specimen, the peaks were the same. Two prominent peaks that are similar to all the investigated alloys occur within the 1026-1032cm^{-1} and 1048-1062cm^{-1} ranges. The peaks were assigned to molecular vibrations of SO_4^{2-} ions. Sulphates form prints in the 900-1250cm^{-1} and 570-680 cm^{-1} range. The Raman peak at 981 cm^{-1} wavenumber is due to the symmetric stretching mode, whilst the Raman peak at 1051 cm^{-1} is as a result of the asymmetric stretching mode [30]. A broad peak at approximately 840cm^{-1} wavenumber is believed to be due to molecular vibrations of SO_4^{2-} ions. Co_3O_4 was detected on the surface of the two Co-containing alloys, Alloy P420 and Alloy P421.

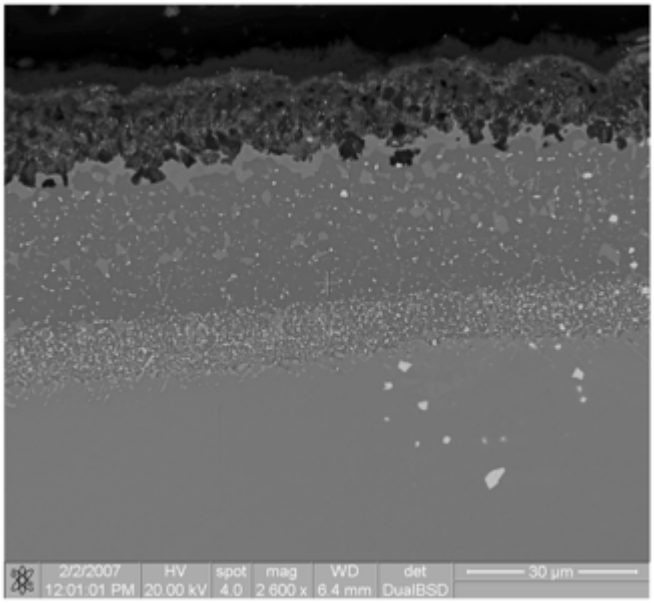

Fig. (6a). Cross-section showing the different phases formed when the coated alloy was exposed to 0.2% SO_2-N_2 atmosphere.

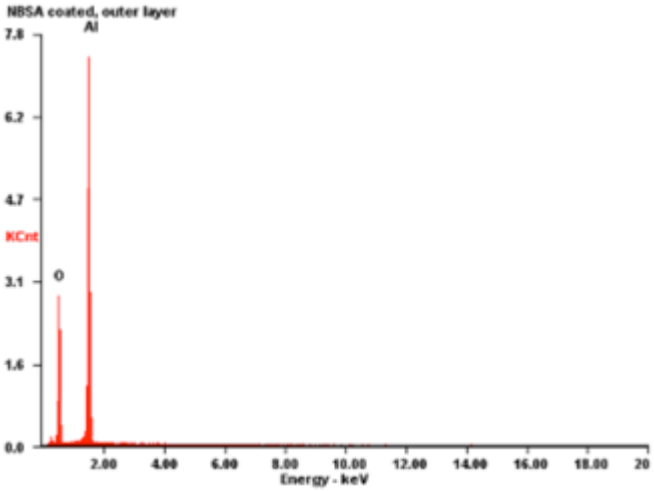

Fig. (6b). EDX analysis of the external scale of the coated alloy after sulphidation.

Pt-Al-Cr-Ru Alloy Group

Peaks that formed on the surface of Alloy RS2 were sharp and had high intensities. Raman spectrum of Alloy RS2 was similar to that of Alloy RS3, as illustrated in Figs. (**9**, **10**). Table **2** shows the peaks that formed on the surface of Alloys RS1, RS2 and RS3.

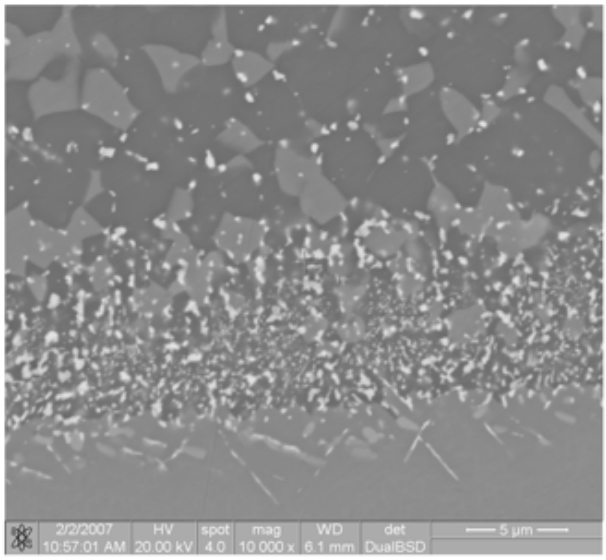

Fig. (7a). Inter-diffusion zone at high magnification of the coated Ni-based superalloy in a 0.2% SO_2-N_2 atmosphere.

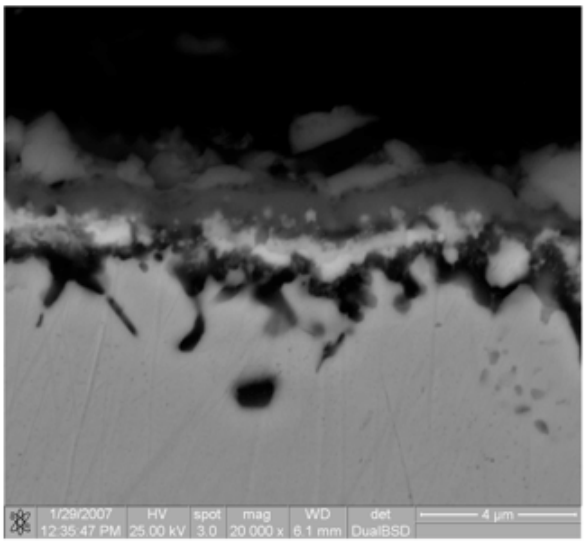

Fig. (7b). Secondary image of the cross-section of the uncoated Ni-based superalloy after sulphidation.

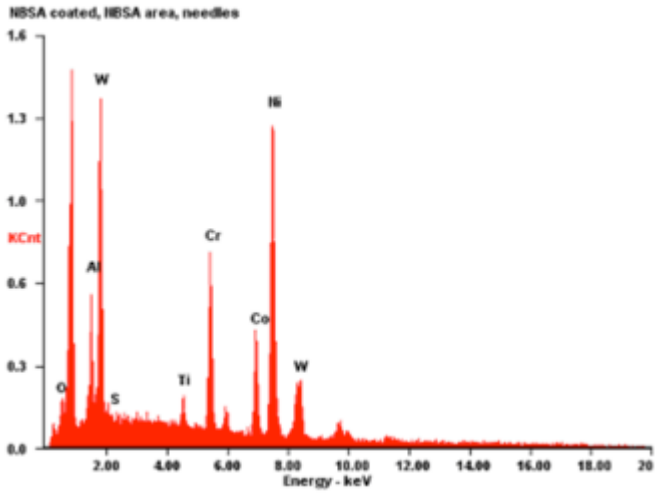

Fig. (7c). EDX analysis of the needle-like phases that formed between the substrate and the coating.

The Pt-Al-Co Alloy Group

The Raman spectra of Alloys P420 and P421 are nearly the same, and the spectra are depicted in Figs. (**11**, **12**). The four peaks at 486, 528, 629 and 699 cm^{-1} wavenumbers were assigned to Co_3O_4 as indicated in Table **3** and compared to cobalt peaks found by Hadjiev and co-workers [30]. The peak at 194.4 cm^{-1} due to F_{2g} vibrations is not observed because the spectral range started at 250cm^{-1}.

The Coated and Uncoated NBSA Group

In a study by Kloproggee and Frost [31], the peaks at 1027 and 1029 cm^{-1} wavenumbers were assigned to N-O-Al bond vibrations. This suggested that traces of nitrates were also formed on the surfaces of the oxidised NBSAs. The results obtained suggest that sulphate salts, with possible traces of nitrates, formed on the surfaces of the alloys.

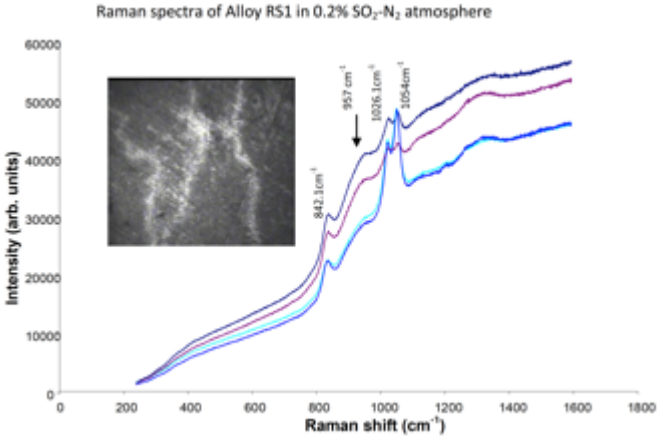

Fig. (8). Raman spectra at different areas on the external surface of Alloy RS1 after sulphidation at 900°C for 60 hours.

Table 2. Raman spectra peak positions from the surface of Pt-based superalloys after exposure to a corrosive gas.

Samples	Peak 1 (cm^{-1})	Peak 2 (cm^{-1})	Peak 3 (cm^{-1})
Alloy RS1	842.1	1026.1	1054
Alloy RS2	834	1027	1056
Alloy RS3	836	1027	1057

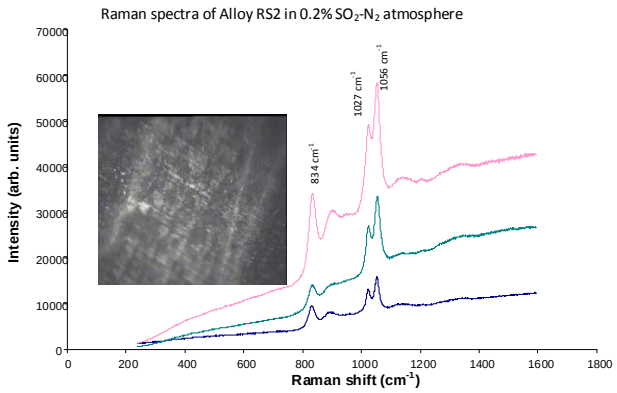

Fig. (9). Raman spectra from different areas on the external surface of Alloy RS2 after sulphidation at 900°C for 60 hours.

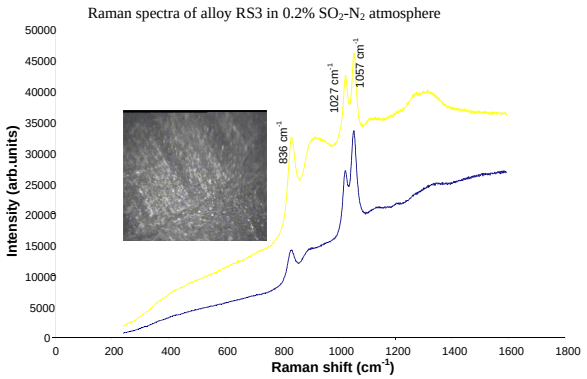

Fig. (10). Raman spectra from the different areas on external surface of Alloy RS3 after sulphidation at 900°C for 60 hours.

Table 3. Comparison of Raman shifts of Co_3O_4 and the corroded alloy P420 exposed to 0.2% SO_2-N_2 corrosive gas at 900ºC.

Vibrational Mode	Hadjiev *et al.* [30] (Co_3O_4)	This Study
F_{2g}	194.4	-
E_g	482.4	486
F_{2g}	521.4	528
F_{2g}	618.4	629
A_{1g}	691	699

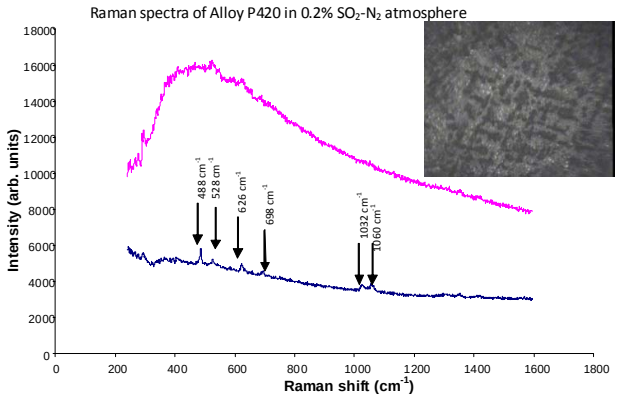

Fig. (11). Raman spectra collected from different areas on the external surface of Alloy P420 after sulphidation at 900°C for 60 hours.

CONCLUSION

The resistance to sulphidation of the alloys with Cr, Ru and a combination of both, were more corrosion-resistant than the group containing Co, while the NBSA group showed much poorer resistance compared to both the Pt-based alloy groups and disintegrated after some time of exposure to the corrosive medium. Pt-based superalloys exhibited better corrosion resistance than NBSAs partly as a result of the formation of a protective Al_2O_3 scale. NBSAs suffered internal sulphidation, forming Cr and Ni sulphide corrosion compounds. Pt-based superalloys alloyed with Co showed poor corrosion resistance as a result of depletion of the beneficial alloying elements. Raman spectra analyses suggest that sulphate salts with possible traces of nitrates formed on the surfaces of the alloys. The Pt-based alloys displayed potential for successful application as high temperature corrosion resistant materials. Due to the drawback of their high density and subsequent weight, the most successful option for future exploration and exploitation would probably be as coatings on suitable substrate materials.

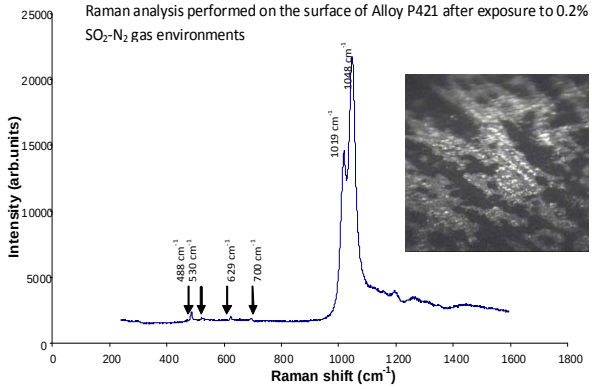

Fig. (12). Raman spectra collected from different areas on the external surface of Alloy P421 after sulphidation at 900°C for 60 hours.

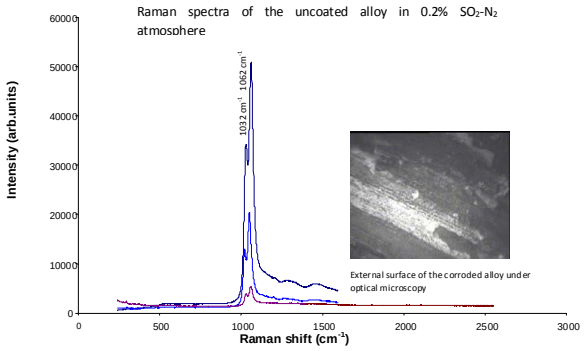

Fig. (13). Raman spectra collected from different areas on the external surface of the uncoated NBSA alloy after sulphidation at 900°C for 60 hours.

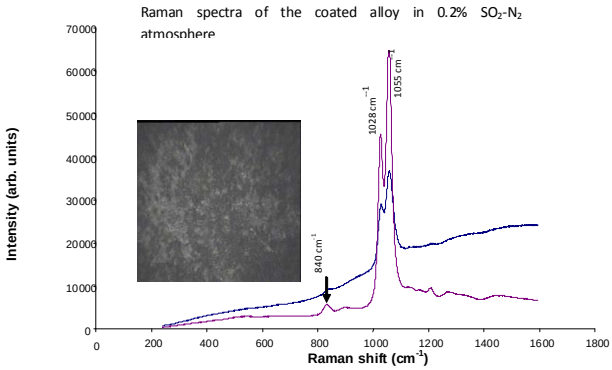

Fig. (14). Raman spectra collected from different areas on the external surface of the coated alloy after sulphidation at 900°C for 60 hours.

CONFLICT OF INTEREST

The authors confirm that this article content has no conflict of interest.

ACKNOWLEDGEMENTS

The authors express their thanks to the NRF/DST Centre of Excellence in Strong Materials, Mintek and the Platinum Development Initiative for financial support to conduct this investigation.

REFERENCES

[1] Elliot P. Practical guide to high-temperature alloys, printed from: Materials Performance, Nickel Development Institute 1990; pp. 1-10.

[2] Sims CT, Stoloff NS, Hagel WC. Superalloys II: High temperature materials for aerospace and industrial power. Wiley-Interscience: New York 1987.

[3] Eliaz N, Shemesh G, Latanision RM. Hot corrosion in gas turbine components. Eng Fail Anal 2002; 9(1): 31-43.

[4] Saltykov P, Fabrichnaya O, Golczewski J, Aldinger F. Thermodynamic modeling of oxidation of Al-Cr-Ni alloys. J Alloys Compd 2004; 381: 99-113.

[5] Sidhu TS, Prakash S, Agrawal RD. Corrosion and performance of nickel-based coatings. Curr Sci 2006; 90(1): 41-7.

[6] Pomeroy M. Coatings for gas turbine materials and long term stability issues. Mater Des 2005; 26: 223-31.

[7] Konter M, Thumann M. Materials and manufacturing of advanced industrial gas turbine components. J Mater Process Technol 2001; 117: 386-90.

[8] Sharafat S, Kobayashi A, Chen Y, Ghoniem NM. Plasma spraying of micro-composite thermal barrier coatings. Vacuum 2002; 65: 415-25.

[9] Yokowaka T, Osawa M, Nishida K, Kobayashi T, Koizumi Y, Harada H. Partitioning behavior of platinum group metals on the γ and γ' phases of Ni-based superalloys at high temperature. Scripta Mater 2003; 49: 1041-6.

[10] Shultz U, Leyens C, Fritsher K, *et al*. Some recent trends in research and technology of advanced thermal barrier coatings. Aerosp Sci Technol 2003; 7(1): 73-80.

[11] Gurrappa I. Identification of hot corrosion resistant MCrAlY based bond coatings for gas turbine engine applications. Surf Coat Technol 2001; 139: 272-83.

[12] Fritscher K, Leyens C, Peters M. Development of a low-expansion bond coating for Ni-base superalloys. Mater Sci Eng A 1995; 190: 253-8.

[13] Vorberg S, Wenderoth M, Fischer B, Glatzel U, Völkl R. A TEM investigation of the γ/γ' phase boundary in Pt-based superalloys. JOM 2005; 57: 49-51.

[14] Pint BA, DiStefano JR, Wright IG. Oxidation resistance: one barrier to moving beyond Ni-base superalloys. Mater Sci Eng A 2006; 415: 255-63.

[15] Süss R, Freund D, Völkl R, *et al*. The creep behaviour of platinum-based γ/γ' analogues of nickel-based superalloys at 1300°C. Mater Sci Eng A 2002; 338: 133-41.

[16] Hüller M, Wenderoth M, Vorberg S, Fischer B, Glatzel U, Völkl R. Optimization of composition and heat treatment of age-hardened Pt-Al-Cr-Ni alloys. Metallurg Mater Trans A 2005; 36: 681-8.

[17] Fisher B, Brehends A, Freund D, Lupton DF, Merker J. High temperature mechanical properties of platinum group metals. Plat Met Rev 1999; 43(1): 18-28.

[18] Coupland DR, Corti CW, Selman GL. The PGM concept: Enhanced resistant superalloys for industrial and aerospace applications: Behaviour of High Temperature Alloys in Metals Society, Proceedings of the International Conference, Petten, (N.H), Netherlands 1979.

[19] Hill PJ, Fairbank GB, Cornish LA. New developments in high-temperature Platinum alloys. JOM 2001; 53: 19-20.

[20] Wolff IM, Hill PJ. Platinum metals-based intermetallic for high temperature service. Plat Met Rev 2000; 44(4): 158-66.

[21] Deb D, Iyer SR, Radhakrishnan VM. Assessment of high temperature performance of a cast nickel base superalloy in corrosive environment. Scripta Mater 1996; 35(8): 947-52.

[22] Carter TJ. Common failures in gas turbine blades. Eng Fail Anal 2005; 12: 237-47.

[23] Sidhu BS, Prakash S. Studies on the behaviour of satellite-6 as plasma sprayed and laser remelted coatings in molten salt environment at 900°C under cyclic conditions. J Mater Process Technol 2006; 172: 52-63.

[24] Cornish LA, Süss R, Völkl R, *et al*. Overview of the development of new Pt-based alloys for high temperature application in aggressive environments. JSAIMM 2007; 107(11): 697-711.

[25] Hill PJ, Cornish LA, Ellis P, Witcomb MJ. The effects of Ti and Cr additions on the phase equilibria and properties of (Pt)/Pt_3Al alloys. J Alloys Compd 2001; 322: 166-75.

[26] Cornish LA, Hohls J, Hill PJ, Prins S, Süss R, Compton DN. The development of platinum based alloys and their thermodynamic database. JSAIMM 2002; 38(3-4): 197-204.

[27] Süss R, Douglas A, Cornish LA. An electron microscope investigation of tensile samples of Pt-based superalloys: Proc. Microsc. Soc. South Africa 34; p. 10. Pretoria, 30th November-3rd December 2004.

[28] Süss R, Hill PJ, Ellis P, Cornish LA. The oxidation resistance of Pt-base superalloy $Pt_{80}Al_{14}Cr_3Ru_3$ compared to that of $Pt_{86}Al_{10}Cr_4$: Proc. Microsc. Soc. South Africa 31; p. 21, Johannesburg, 5th-7th December 2001.

[29] Chown LH, Cornish LA, Joja B. Structure and properties of Pt-Al-Co alloys: Proc. Microsc. Soc. South Africa 2004; 34: 11.

[30] Hadjiev VG, Illiev MN, Vergolov IV. Raman spectra of Co_3O_4. J Phys Chem: Sol State Phys 1988; 21: 199-201.

[31] Kloproggee JT, Frost RL. Raman microscopy study of basic aluminium sulphate. J Mater Sci 1999; 34: 4199-202.

Received: June 14, 2013 Revised: December 18, 2013 Accepted: February 21, 2014